Smoothed Particle Hydrodynamics Simulations for Hysteretic Behaviours of Capillary Interactions

Yanyao Bao, Ling Li, Luming Shen, and Yixiang Gan*

School of Civil Engineering, The University of Sydney, NSW 2006, Australia
*Corresponding author's E-mail: yixiang.gan@sydney.edu.au

Abstract

Dynamic wetting and dewetting behaviours in multiphase flow have a significant influence on many geotechnical applications, such as unsaturated soil mechanics, carbon geosequestration, and oil recovery. In this paper, a smoothed particle hydrodynamics (SPH) method with an inter-particle force formulation is applied to simulate capillary interactions, involving surface tension and dynamic contact angle effects. In particular, the frictional boundary condition at liquid-solid interface is critical in dynamic simulations, while the traditional treatment requiring arbitrary friction or dragging force can neither reflect the complex interaction between different phases nor contain direct links to physical quantities. Therefore, we introduced an interfacial viscous force in the SPH to replicate realistic dynamic behaviour of fluid-solid interactions. The interface of fluids with different surface tension and wettability between different phases can be reproduced by adjusting liquid-liquid and liquid-solid inter-particle force parameters respectively. Through parametric studies, other physical properties predicted from the model including density, viscosity and compressibility are also implemented and can be altered for various constituents. The capillary tube scenario was studied, containing fluid particles with shifting substrate to generate wetting and dewetting phenomena. Dynamic contact angles were recorded under different moving speeds of the contact line. After analysing results from different moving speeds, the dynamic contact angles and corresponding capillary numbers can be correlated by a power law. This result is in a good agreement with the experimental observations under dynamic loading conditions. The simulations have demonstrated that the proposed numerical model accounts for the pore-scale effects, including dynamic contact angle and surface tension, and can be used for simulating multiphase flow in geomaterials.

Keywords: Smoothed particle hydrodynamics, multiphase flow, surface tension, capillary number, contact angle dynamics.

1. INTRODUCTION

Complex interactions among gas, liquid and solid phases in unsaturated geomaterials are of significant importance in many geoenvironmental applications, such as groundwater contamination, landslides, oil recovery, and carbon sequestration (Sorbino and Nicotera 2013, Zhao et al 2016). Rate-dependent wetting and dewetting effects play a substantial role in understanding the multiphase behaviours of porous media and can thus further shed light on identifying solutions to these abovementioned problems. A number of experimental studies and theoretical models suggested that the apparent contact angle varies with the velocity of moving contact line (Schäffer and Wong 2000). However, the experimental findings are limited by the available experimental conditions and facilities. With this consideration, the

numerical approach is used as a powerful tool to study the capillary interactions and investigate the fundamental mechanisms.

In this study, a smoothed particle hydrodynamics (SPH) model is employed to simulate dynamic contact angle in a capillary tube at pore scale. A particle-particle interaction with short range repulsive and long range attractive force has been adopted to generate the surface tension effects and various contact angles. Moreover, an interfacial viscous force is implemented between the liquid-solid interface to modify the tangential boundary condition from smooth to friction. The capacity of the model is demonstrated by accurately simulating a wide range of surface tension and contact angles as well as the frictional boundaries. Then, dynamic advancing or receding contact angles are simulated by rising up or pulling down, respectively, the bottom substrate of the capillary tube with different speeds. By analysing the corresponding relations between the moving contact line velocity and contact angle, an empirical equation is obtained for describing dynamic contact angle under a wide range of capillary number Ca.

2. NUMERICAL MODELS

1.1. Governing Equations

For an incompressible Newtonian fluid, the Lagrangian form of Navier-Stokes equation reads as

$$\frac{d\boldsymbol{v_i}}{dt} = -\frac{\nabla P}{\rho_i} + \mu\frac{\nabla^2\boldsymbol{v_i}}{\rho_i} + \boldsymbol{F} \tag{1}$$

where $\boldsymbol{v_i}$ is flow velocity, P is pressure, ρ is fluid density, $\mu\frac{\nabla^2\boldsymbol{v_i}}{\rho_i}$ is viscous term, and $\boldsymbol{F}$ corresponds to total volumetric force acting on unit mass. To represent the conservation of mass of fluid flow, the continuity equation is usually written in the following form:

$$\frac{d\rho}{dt} = -\rho\nabla\cdot\boldsymbol{v}_i \tag{2}$$

We approximate the incompressibility of fluids using the weakly-compressible approach by applying a stiff equation of state with the form stated in Becker and Teschner (2007) as

$$P = \frac{c^2\rho_0}{\gamma}\left[\left(\frac{\rho}{\rho_0}\right)^{\gamma} - 1\right] \tag{3}$$

where c is artificial speed of sound, ρ_0 is reference density, and γ is equation parameter. In this work, we choose the artificial speed of sound as $c > 10V_{max}$ along with $\gamma = 7$, where V_{max} is the expected maximum particle velocity (Monaghan JJ 1994, Becker M and Teschner M 2007).

1.2. SPH Discretisation and Inter-Particle Force

The SPH method is based on the idea that a continuous field $A(\boldsymbol{r})$ at position $\boldsymbol{r}$ can be smoothed by a convolution integral with a smoothing function or smoothing kernel, $W(\boldsymbol{r}-\boldsymbol{r}', h)$, allowing the value of any function to be obtained at a given point considering its neighbouring points as

$$A(\boldsymbol{r}) = \int_{\Omega} A(\boldsymbol{r}')W(\boldsymbol{r}-\boldsymbol{r}', h)d\boldsymbol{r}' \tag{4}$$

where $A(\boldsymbol{r})$ is the smoothed field, $\boldsymbol{r}'$ is radius vector, Ω is the volume of the integral that contains $\boldsymbol{r}$, h is smoothing length, and function $W(\boldsymbol{r}-\boldsymbol{r}', h)$ should satisfy the conditions explained in Monaghan (1992). The integral in Equation 4 is cast in discrete form for computational use as

$$A(\boldsymbol{r}_i) = \sum_j A(\boldsymbol{r}_j)\frac{m_j}{\rho_j}W(\boldsymbol{r}_i-\boldsymbol{r}_j, h) \tag{5}$$

In this study, a Gaussian kernel is used in this SPH model to improve accuracy of smoothing. The density of a fluid particle i is calculated via summation over all its neighbor particles j, i.e., $\rho_i = \sum_j m_j W(\boldsymbol{r}_{ij}, h)$. The pressure driven part of the momentum equation is implemented following the approach proposed by Monaghan (1992), in which the pressure gradient is symmetrised by rewriting $\nabla P/\rho$ in Equation 1 to ensure momentum conservation. For the viscous term, a Monaghan style artificial viscosity model is implemented to stabilise the numerical algorithm. The time step Δt is set to satisfy the constraint detailed in Morris et al (1997).

Furthermore, an inter-particle force formulation proposed by Li et al. (2017) is applied to reproduce the interfacial properties, including the surface tension and wettability between different phases. In their work, pair potential energy is constructed by a linear combination of cubic splines. The resulted short range repulsive and long-range attractive particle-particle interaction force can be adjusted to reproduce surface tension and wetting behaviours. In addition, to prevent the unphysically penetration of liquid particles into the solid particles, additional repulsive boundary forces are added on fluid particles similar to those implemented in Monaghan and Kajtar (2009).

1.3. Frictional boundary conditions

In most SPH simulations, the boundaries of rigid bodies have been prescribed with different mechanisms, such as ghost particles, fluid particles, and boundary particle forces (Monaghan and Kajtar 2009). However, all the above methods are only appropriate for perfectly smooth boundaries, i.e., no net tangential force with respect to the relative motion between solid and fluid SPH particles. In this work, considering the force balance of particle-particle interaction at liquid-solid interface, the net force of short range repulsive and long range attractive force acting on one liquid particle is approximately zero in the tangential direction, as shown in Figure 1. Thus, the surface of the simulated solid boundary is perfectly smooth, ignoring a thin boundary layer ($L_0/2$) of liquid under shearing when a relative tangential motion is present at the interface. In order to implement the frictional boundary condition, we introduce a new

algorithm which imposes a viscous force, $\boldsymbol{F}_l^{vis}$, on the liquid particles that directly contact with the solid phase as

$$\boldsymbol{F}_l^{vis} = A \cdot \tau = L_0 \cdot \eta \cdot \dot{\gamma} \tag{6}$$

where A is liquid-solid interface area (per particle interaction), in 2D case being the length of particle spacing L_0, τ is shear stress, η is the viscosity of fluid, and $\dot{\gamma}$ is shear rate. In principle, the parameter η in Equation 6 should equal to the bulk viscosity of fluid for the stick condition. However, in this slip contact scenario, viscosity at interface would be smaller than bulk viscosity. Therefore, η is replaced by η^* which has a different value depending on the actual flow profile within the boundary layer. Finally, we have interfacial viscous force implemented with the following form:

$$\boldsymbol{F}_l^{vis} = \begin{cases} -L_0 \cdot \eta^* \cdot \frac{\boldsymbol{v}_l - \boldsymbol{v}_s}{\frac{L_0}{2}}, & r_{ls} \leq L_0^S \\ 0 & r_{ls} > L_0^S \end{cases} \tag{7}$$

where $\boldsymbol{v}_l$-$\boldsymbol{v}_s$ is the relative velocity of liquid and solid particles, and L_0^S is the smoothing length for $\boldsymbol{F}_l^{vis}$.

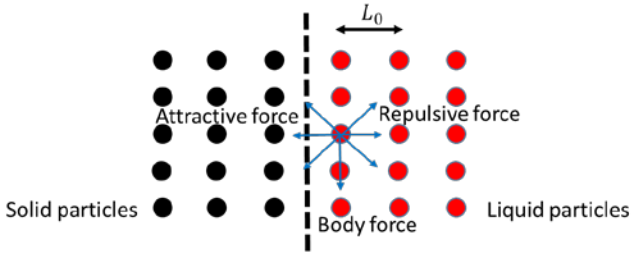

Figure 1. Schematic drawing for the force balance of fluid particle at the solid-liquid interface.

3. RESULTS AND DISCUSSION

In this section, after validating the surface tension effect, the significance of interfacial viscous force is demonstrated by conducting capillary tube simulations with and without the viscous force. Next, dynamic behaviour of contact angle is studied and the correlation between the dynamic contact angles and capillary number is derived.

1.1. Validating Surface Tension

To examine the surface tension scheme used in this study, the evolution of a 2D droplet with zero gravity in vacuum is modelled. The simulation is conducted with the condition in which a square droplet (l = 1 mm) with density of 1000 kg/m^3 and surface tension coefficient of 0.073 N/m. It can be seen in Figure 2 that, the shape of the droplet transforms from square to round due to the surface tension effect. More details about this implementation can be found in Li et al. (2017). This SPH scheme is then used for the dynamic contact angle simulations.

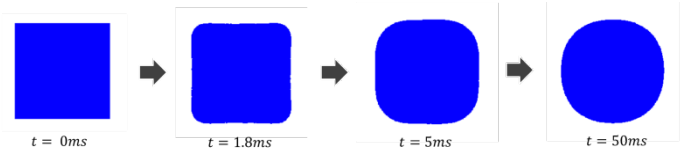

Figure 2. Shape evolution of a water droplet with zero gravity.

1.2. Dynamic Contact Angle

A number of empirical relationships and theoretical models for dynamic wetting and dewetting have been discussed in the literature, expressing the dynamic contact angle θ_d as a function of the capillary number Ca and the quasi-static advancing/receding contact angle $\theta_{a/r}$ during spreading. For $\mathrm{Ca} < 10^{-2}$, the most commonly suggested relationship is (Schäffer and Wong 2000)

$$\left|\cos\theta_{a/r} - \cos\theta_d\right| = A\mathrm{Ca}^B \tag{8}$$

where A and B are constants, the non-dimensional number Ca is defined as the ratio between viscous and interfacial forces as

$$\mathrm{Ca} = \eta v/\alpha \tag{9}$$

where v is the contact line velocity, α is the surface tension, and η is the viscosity of the liquid.

In order to study the dynamic contact angle behaviours, a 2D capillary tube with a moving substrate, shown in Figure 3, is modelled in vacuum with the following parameters. The size of the capillary tube is 4 mm × 1.36 mm and the domain of fluid is 1.8 mm × 1.2 mm. The resolution L_0 for both liquid and solid particle is 0.025 mm. The fluid is simulated with density of 997 kg/m^3, surface tension coefficient of 0.073 N/m, viscosity of 0.1 Pa·s, and interfacial viscous force parameter of 0.002 Pa·s. The time step Δt is 4.15×10^{-7} s and the gravity acceleration is 9.81 m/s^2. The capillary tube is under stable condition before bottom substrate start moving. The bottom substrate moves along the vertical direction at a speed ranging from 0.002 mm/s to 20 mm/s.

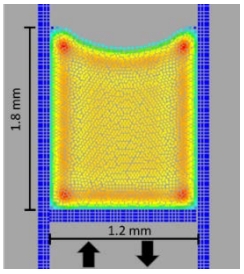

Figure 3. Capillary tube with a moving substrate.

All simulations started with same initial configuration under stable status of the capillary tube system. The contact angle was measured by fitting the liquid surface at the triple line region throughout the dynamic process. The dynamic advancing and receding angle (θ_d^{adv} and θ_d^{rec}) is obtained by pushing up and dragging down the substrate at different velocity, and the quasi-

static advancing and receding contact angles (θ_s^{adv} and θ_s^{rec}) is obtained with extremely slow velocity of 0.0002 mm/s.

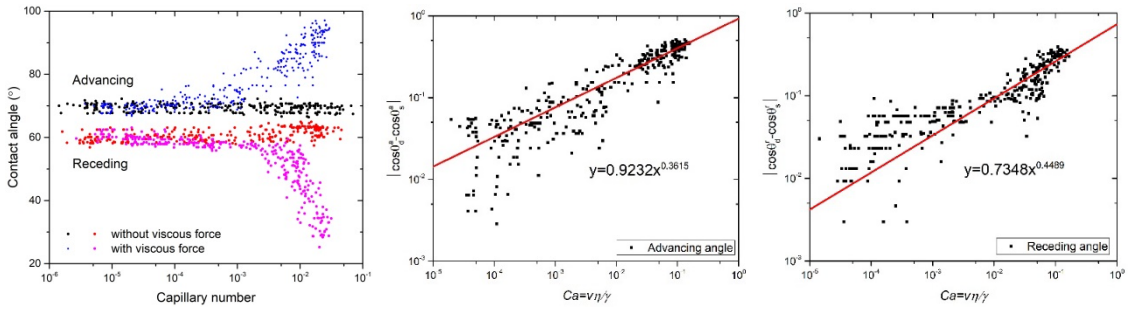

(a) (b) (c)

Figure 4. (a) Simulations of dynamic contact angle with and without the interfacial viscous force; (b) Power law fitting of advancing case; (c) Power law fitting of receding case

The effectiveness of interfacial viscous force $\boldsymbol{F}_l^{vis}$ is investigated by conducting two series of dynamic simulations shown in Figure 4(a). In the case of no viscous force is incorporated, no rate dependent behaviour of dynamic contact angle is observed. After adding $\boldsymbol{F}_l^{vis}$ in the inter particle force model, the contact angles are shown to be varied with the velocity of moving contact line. The correlation between the dynamic contact angle and capillary number is plotted in log-log scale as shown in Figure 4(b) and (c). The quasi-static advancing and receding angles are 67.31° and 62.63°, respectively. The dynamic advancing angle ranges from 69.27° to 94.53° with the increase of moving contact line velocity and 38.33° to 60.77° for dynamic receding angles. The capillary number Ca ranges between 10^{-5} and 10^{-1}. Based on Equation 9, two power-law fitting curves are derived for advancing and receding case, respectively. The values of parameter B in this study, 0.3615 and 0.4489, is in good agreement compared with experimental results and theoretical predictions, which usually ranges from 0.4 to 0.7 (Ishimi et al 1986, Stokes et al 1990, Ström et al 1990). Note, the case without the newly introduced interfacial viscous force shows almost no dependency on Ca, i.e., B≈0. This quantitative agreement demonstrated that our model has the ability to successfully reproduce the rate-dependent behaviour of moving contact line as well as the potential to predict dynamic advancing/receding angle.

4. CONCLUSION

In this study, we introduce an interfacial viscous force into multiphase SPH numerical scheme to capture the rate-dependent wetting and dewetting phenomena. This numerical scheme is employed to simulate static and dynamic behaviours of contact angle in a capillary tube under different flow rates. An empirical correlation between capillary number and dynamic contact angle is established and share good agreements with experimental findings and theoretical analysis. These preliminary numerical results demonstrated the potential of using this proposed method for accounting the pore-scale effects, including the hysteretic contact angle, and for simulating multiphase flow in geomaterials under dynamic conditions.

REFERENCES

Becker M, Teschner M (2007). Weakly compressible SPH for free surface flows. Proceedings of the 2007 ACM SIGGRAPH/Eurographics symposium on Computer animation. Eurographics Association.

Ishimi K, Hikita H, Esmail, M. (1986). Dynamic contact angles on moving plates, AIChE Journal, 32(3), 486-492.

Monaghan JJ (1992). Smoothed particle hydrodynamics, Annual review of astronomy and astrophysics, 30(1), 543-574.

Monaghan JJ, Kajtar JB (2009). SPH particle boundary forces for arbitrary boundaries, Computer Physics Communications, 180(10), 1811-1820.

Morris JP, Fox PJ, Zhu Y (1997). Modeling low Reynolds number incompressible flows using SPH, Journal of Computational Physics, 136(1), 214-226.

Schäffer E, Wong PZ (2000). Contact line dynamics near the pinning threshold: A capillary rise and fall experiment, Physical Review E, 61(5), 5257.

Sorbino G, Nicotera MV (2013). Unsaturated soil mechanics in rainfall-induced flow landslides, Engineering Geology, 165, 105-132.

Stokes J, Higgins M, Kushnick A, Bhattacharya S, Robbins MO (1990). Harmonic generation as a probe of dissipation at a moving contact line, Physical review letters, 65(15), 1885.

Ström G, Fredriksson M, Stenius P, Radoev B (1990). Kinetics of steady-state wetting, Journal of colloid and interface science, 134(1), 107-116.

Zhao B, MacMinn CW, Juanes R (2016). Wettability control on multiphase flow in patterned microfluidics, Proceedings of the National Academy of Sciences, 113(37), 10251-10256.

Li L, Shen L, Nguyen, GD, El-Zein A, Maggi F, (2017). A generalised smoothed particle hydrodynamics framework for modelling multi-phase interaction, submitted to Computational Mechanics.